



HAL
open science

Basin-scale 3D modelling of the northern Upper Rhine Graben: insights into basement fault-related geothermal flow pathways

Adriana Lemgruber-Traby, Claire Bossennec, Gillian Béthune, Christine Souque, Renaud Divies, Jeroen van der Vaart, Kristian Bär, Ingo Sass

► To cite this version:

Adriana Lemgruber-Traby, Claire Bossennec, Gillian Béthune, Christine Souque, Renaud Divies, et al.. Basin-scale 3D modelling of the northern Upper Rhine Graben: insights into basement fault-related geothermal flow pathways. *GEOENERGY*, 2023, 1 (1), 10.1144/geoenergy2023-002. hal-04503257

HAL Id: hal-04503257

<https://ifp.hal.science/hal-04503257v1>

Submitted on 13 Mar 2024

HAL is a multi-disciplinary open access archive for the deposit and dissemination of scientific research documents, whether they are published or not. The documents may come from teaching and research institutions in France or abroad, or from public or private research centers.

L'archive ouverte pluridisciplinaire **HAL**, est destinée au dépôt et à la diffusion de documents scientifiques de niveau recherche, publiés ou non, émanant des établissements d'enseignement et de recherche français ou étrangers, des laboratoires publics ou privés.



Distributed under a Creative Commons Attribution 4.0 International License

Basin-scale 3D modelling of the northern Upper Rhine Graben: insights into basement fault-related geothermal flow pathways



Adriana Lemgruber-Traby¹, Claire Bossennec², Gillian Béthune¹, Christine Souque¹, Renaud Divies¹, Jeroen van der Vaart², Kristian Bär² and Ingo Sass^{2,3}

¹ IFP Energies Nouvelles, 1–4 Avenue du Bois Préau, 92852, Rueil Malmaison, France

² Institute of Applied Geosciences, Geothermal Science and Technology, Technische Universität Darmstadt, Schnittspahnstraße 9, 64287 Darmstadt, Germany

³ Section 4.8: Geoenergy, GFZ German Research Centre for Geosciences, Wissenschaftspark ‘Albert Einstein’, Telegrafenberg, 14473 Potsdam, Germany

AL, 0000-0002-5462-7058

*Correspondence: adriana.traby@ifpen.fr

Present address: KB, Vulcan Energy Subsurface Solutions GmbH, An der RaumFabrik 33C, 76227 Karlsruhe, Germany

Abstract: A regional assessment of the potential for geothermal heat production, power generation and also heat storage requires an evaluation of the heat in place and its recharge. Both are controlled by the flow properties and natural fluid flow through the reservoir at the present day, which must be thoroughly analysed based on the understanding and modelling of the architecture of deep reservoirs. In the Upper Rhine Graben, well known for its vast geothermal potential, a characterization of the structural organization at the basin scale and an understanding of mass and heat transfer are, therefore, useful for correctly estimating the technical and economic potential for geothermal energy. The distribution of the resources can be quantified based on the basin analysis approach. This is classically used for hydrocarbon resources and is applied in this study to predict the geothermal fluid-flow paths. The role of faults and their hydraulic regime on temperature field heterogeneities is investigated. Several scenarios with or without rift basin internal faults and various transmissivity ranges along these faults are analysed and compared. The measured temperature field is used for the calibration of the different model scenarios results. The scenario with the most significant role for internal faults as fluid-flow pathways in the western Upper Rhine Graben is the one that provides the most accurate reproduction of the temperature field. Such output highlights the importance of quantifying the hydraulic behaviour of faults and associated fracture networks in space and time.

Supplementary material: dataset containing geometry, facies distribution and main results of scenario 4 is available at <https://doi.org/10.6084/m9.figshare.c.6628506>

Received 20 January 2023; revised 26 April 2023; accepted 3 May 2023

Geothermal resource assessment and reserve estimation are strongly linked to an understanding of fluid-flow pathways. Through its impact on the thermal structure of the subsurface, on the heat recharge and on the distribution of elements like lithium, fluid flow defines and thus impacts the decision-making processes in geothermal reservoir exploration (Bär 2012; Bär and Sass 2014). Fluid and heat flow should be understood and quantified numerically, and such numerical approaches can be seen to be widespread in previous research (Guillou-Frottier *et al.* 2013; Freyemark *et al.* 2017, 2019; Torresan *et al.* 2021). The integrative geological basin-scale approach workflow proposed in this study allows an analysis of the thermal resource, including the effects of the fault network on the fluid flow and temperature fields. This is made possible thanks to algorithms and numerical tools implemented in basin modelling that allow modelling and mapping of volumes affected by thermal anomalies and their evolution through geological time (Ungerer *et al.* 1990; Schneider *et al.* 2000; Hantschel and Kauerauf 2009; Peters *et al.* 2017; Lemgruber-Traby *et al.* 2020a, b). The integration of fault-system geometries and the possibility of tuning fault parametrization is beneficial in quantifying the impact of fault properties on the modelled temperature field (Guillou-Frottier *et al.* 2013, 2020).

The Upper Rhine Graben is a geothermal system where the fault pattern controls thermal anomalies (Baillieux *et al.* 2013, 2014; Armandine Les Landes *et al.* 2019; Freyemark *et al.* 2019; Koltzer *et al.* 2019a; Reinecker *et al.* 2019; Bär *et al.* 2020). Indeed, about

80% of thermal anomalies are linked to fluid flow at the basin scale, both in the sedimentary basin and in the underlying basement, and the remaining 20% is explained by radiogenic heat production within the crystalline basement (Baillieux *et al.* 2014; Freyemark *et al.* 2017; Armandine Les Landes *et al.* 2019). This study aims to implement a geothermal system in a basin model (Ungerer *et al.* 1990; Lemgruber-Traby *et al.* 2020a) to decipher specific points regarding the role of advective and convective heat transfer, and to constrain faults and how their parametrization affects the potential of the top basement and overlying sedimentary layers that are targeted in different part of the graben. This three-dimensional and basin-scale approach also allows testing of, in a 3D framework, the previously proposed 2D conceptual models of fluid pathways in faulted deep-seated geothermal reservoirs (Bossennec *et al.* 2021a, b) present in continental rift systems. Finally, it opens up the possibility of integrating the hydrothermal fluid circulation history in future studies with the aim of accessing the minerals mobilized by and circulated with the brine.

Geological context

Structural settings of the northern Upper Rhine Graben

The northern Upper Rhine Graben (NURG) is the most northern segment of the Upper Rhine Graben (URG). Part of the European Cenozoic Rift System (ECRIS) (Ziegler 1992; Sissingh 1998; Derer

et al. 2005), the URG is a typical example of intracontinental rifting. This NNE-striking graben is bordered to the north by the Hünsrück–Taunus Rhenohercynian massif. The 300 km-long URG extends southwards to the Alpine Jura, with an east–west width of 30–40 km. The southern limit of the NURG is determined by a structural Hercynian high below Strasbourg (Schumacher 2002; Lopes Cardozo and Behrmann 2006). The NURG constitutes one of the sub-basins segmenting the URG. These sub-basins are controlled by pre-existing Variscan structuration (Bertrand *et al.* 2018) affecting the basement (Edel *et al.* 2007; Skrzypek 2011). The Vosges and Rheinland Pfalz mountains ('Pfälzer Wald') border the basin on the west. The eastern border fault delimits the URG from the crystalline Odenwald and Schwarzwald massifs (Fig. 1a). The area is affected by a complex fault pattern, presenting first-order structuration with NNE–SSW-orientated faults. The secondary faults strike mainly N000°E, N040°E, N120°E and N150–N170°E (Illies 1972; Schumacher 2002; Lopes Cardozo and Behrmann 2006). A triple porosity fluid-flow system in deep sandstone geothermal reservoirs is often proposed (Haffen *et al.* 2015; Bossennec 2019), while porosity and permeability controlled by fractures and faults are considered in the basement (Gentier *et al.* 2010; Armandine Les Landes *et al.* 2019).

The sedimentology and complex fault pattern are closely related to the multiphased basin development history. Lying on Hercynian basement, the deeper part of the URG corresponds to the eastern part of the Paris Basin. These Permian–Jurassic pre-rift sediments include the main geothermal target in the central and southern parts of the URG – the Buntsandstein Formation. No Cretaceous units are observed in the basin but they were probably deposited and then eroded during a regional uplift in latest Cretaceous and Paleocene times (Ziegler 1987; Schumacher 2002; Böcker *et al.* 2017). This uplift was more important in the northern URG, where Permian–Jurassic pre-rift sediments were also eroded. The latest development phase of the URG was contemporaneous with the Pyrenean and Alpine collision phases (Schumacher 2002), and started, in the Middle Eocene, with a rift phase characterized by regional uplift and volcanism NW from the central URG (Lutz *et al.* 2010, 2013). Concomitant to this tectonic activity, early rift mini-basins with a NE–SW orientation were filled by siliciclastic detrital sediments evolving laterally into clay-limestones layers towards the basin depocentres (Berger *et al.* 2005; Lopes Cardozo and Behrmann

2006; Roussé 2006). During the Middle Eocene the size of the basins increased, followed by an increase in the subsidence rate in the Late Eocene. A regional WNW–ESE extensional regime marked the Oligocene, and the URG then entered a thermal subsidence phase (Schumacher 2002; Meulenkamp and Sissingh 2003; Berger *et al.* 2005) in which the Eocene basins merge into a single large basin (Böcker *et al.* 2017). The regional stress regime then changed to transpressive sinistral shear in the Late Oligocene and Miocene, which gradually uplifted the southern URG during the Burdigalian (Roussé 2006; Timar-Geng *et al.* 2006; Dresmann *et al.* 2010; Roussé *et al.* 2016). This uplift was caused by a lithosphere folding event (Dèzes *et al.* 2004; Berger *et al.* 2005; Bourgeois *et al.* 2007; Ziegler and Dèzes 2007; Reicherter *et al.* 2008) that reactivated NE-striking basement faults (Rotstein *et al.* 2006; Edel *et al.* 2007; Rotstein and Schaming 2008). The Miocene uplift gave the URG a geometry that was close to its current one and was accompanied by considerable regional erosion of late Oligocene sediments in its southern part. The depocentre of the basin, with its maximum subsidence, is located in the northern part of the URG, in the Heidelberg–Mannheim Graben (Schumacher 2002). The NURG underwent a third phase of subsidence from the Pliocene to the Quaternary (Schumacher 2002; Dèzes *et al.* 2004; Cloetingh *et al.* 2006).

Thermal field properties

The present heat flow in the NURG varies from about 70–80 mW m⁻² up to 150 mW m⁻² (Lucazeau and Vasseur 1989; Baillieux *et al.* 2013, 2014). The temperature field at a depth of 2000 m is marked by high-temperature anomalies exceeding 150°C (Aquilina *et al.* 2000; Pribnow and Schellschmidt 2000; Guillou-Frottier *et al.* 2013; Freymark *et al.* 2019). Investigating the basement properties that led to these thermal anomalies is of crucial importance. Positive thermal anomalies observed on isotherm maps exhibit concentric patterns around fault zones (Baillieux *et al.* 2014; Vidal and Genter 2018; Glaas *et al.* 2021). The thermal profiles at Soultz (Vidal *et al.* 2015; Vidal and Genter 2018) exemplify the vertical profiles of these thermal anomalies. They present two zones where the conductive regime dominates: between a depth of 0 and 1 km, corresponding to the middle Triassic and overlying sedimentary layers; and at a depth of 3.5–5 km, when the deep unaltered granite

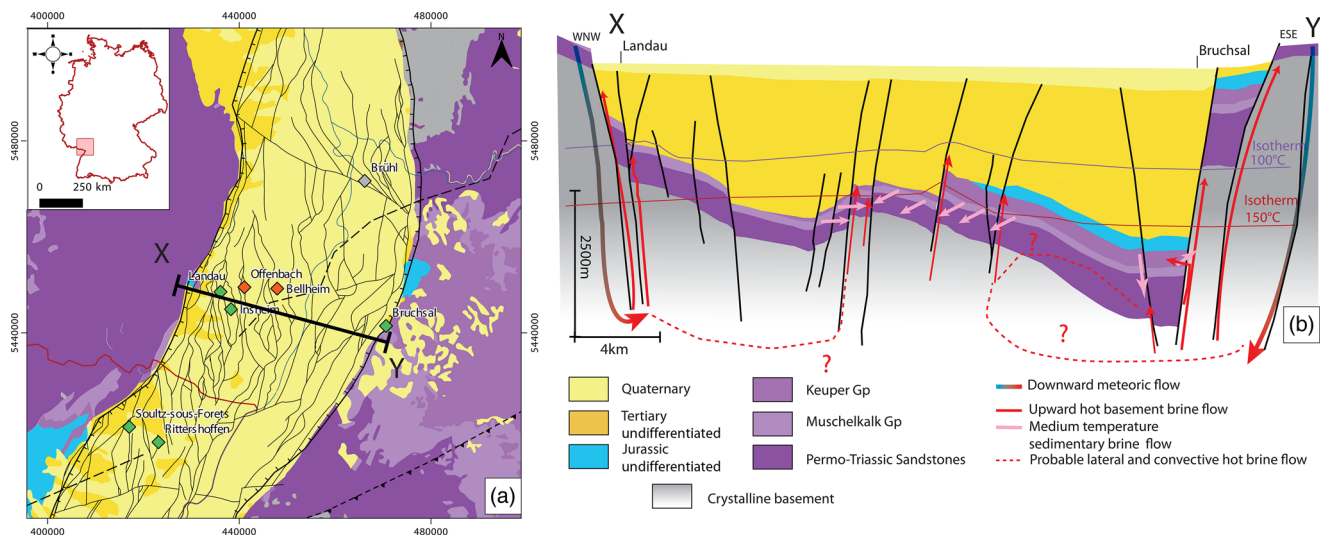


Fig. 1. Geological context of the northern Upper Rhine Graben (NURG). (a) Simplified geological map of the NURG, with a projection of the fault pattern of the top Buntsandstein Group. The minimap on the top left shows the study area (red box) at the border with France and Germany (red line). (b) Cross-section X–Y of the Upper Rhine Graben between Landau and Bruchsal, adapted from Beccaletto *et al.* (2010). Speculated flow pathways from shoulder charge and intra-basin fluid directions in the current rift settings are represented. Sources: Cathelineau and Boiron (2010), Dezayes and Lerouge (2019), Bossennec *et al.* (2021a) and Dezayes *et al.* (2013, 2021).

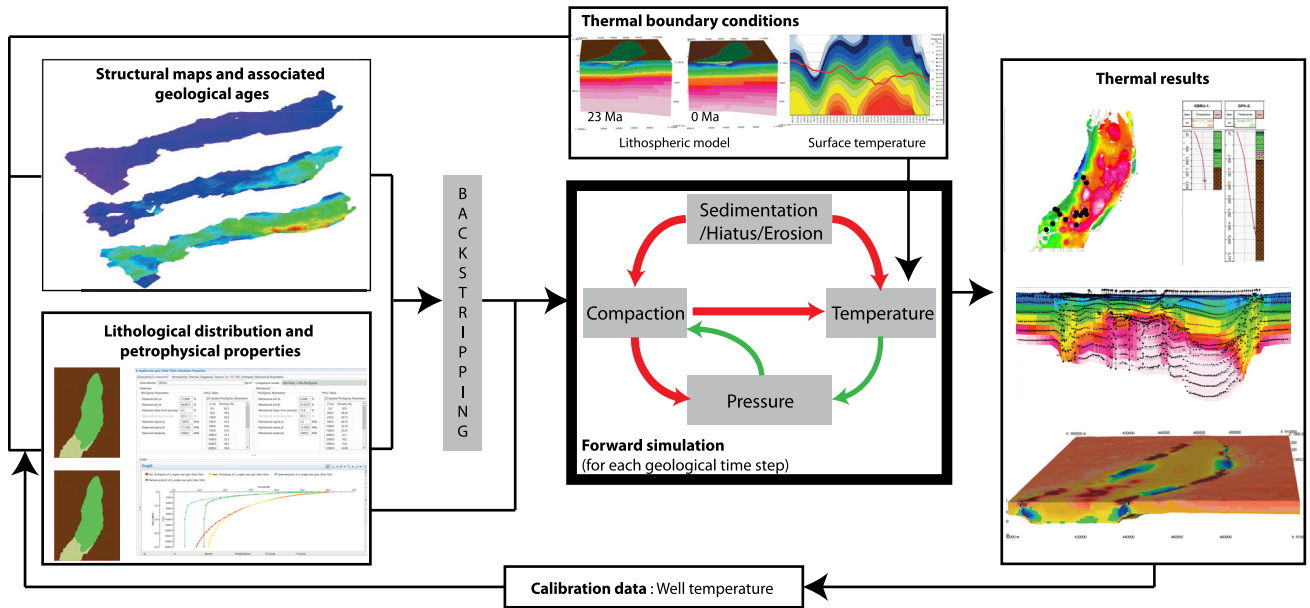


Fig. 2. Basin modelling workflow implementing the geological model, the boundary conditions, the processes involved in the solver and the calibration datasets.

is encountered in the wells. These two conductive intervals are separated by an intermediate zone (1.5–3.3 km) where advection and convection dominate. An almost zero geothermal gradient has been measured in the advective interval, implying a constant temperature of 150°C, in the faulted and altered top basement.

Fluid pathways used by geothermal brines

As summarized in previous studies (Freyemark *et al.* 2017, 2019; Bossennec *et al.* 2021a), heterogeneity of the thermal field and brine composition affect the joint geothermal potential and Li-prone geothermal targets. This observation highlights the importance of fluid pathways in the basement and the deep-basin sediment

advective interval. Fluid pathways are currently controlled at the basin scale by fault zones and shoulder-induced hydraulic gradients (Freyemark *et al.* 2017, 2019). Meteoric waters likely to infiltrate onto topological highs (Rheinland Pfalz, Odenwald, Schwarzwald and Vosges massifs) and develop shoulder convection are usually represented on east–west sections (Fig. 1b). According to the geochemistry and analysis of fluid inclusions, the main reservoir for the hot brine feeding the geothermal sites would be situated in the eastern part of the graben, where the Permo-Triassic sandstones reach depths of more than 4 km and temperatures reach 225°C (Sanjuan *et al.* 2010, 2008; Dezayes *et al.* 2015; Koltzer *et al.* 2019a). These hot brines migrate from the graben centre to the northwestern edge, infiltrate the granitic basement, mix with

Table 1. Petrophysical properties of the models lithofacies types, including solid density (ρ_m), specific surface area (S), vertical permeability multiplier (Zanis), rock matrix thermal conductivity (λ_m) and radiogenic heat production (rhp)

Lithology input in the model	Index	ρ_m (kg m ⁻³)	S (1/m)	Zanis*	λ_m (W m ⁻¹ °C ⁻¹)	rhp (W m ⁻¹)	Source
Marl	1	2675	2.5×10^7	0.1	2.76	1.3×10^{-6}	TemisFlow software lithology library
Shale lacustrine	24	2645	2.0×10^7	0.01	2.37	19.0×10^{-7}	TemisFlow software lithology library
Sandstones deltaic	25	2665	2.0×10^6	0.7	4.6	9.5×10^{-7}	TemisFlow software lithology library
Undifferentiated lacustrine facies	26	2645	2.0×10^7	0.01	2.37	19.0×10^{-7}	TemisFlow software lithology library
Fluvio-lacustrine	25	2665	2.0×10^6	0.7	4.6	9.5×10^{-7}	TemisFlow software lithology library
Lacustrine limestones	27	2710	5.0×10^5	1	3.57	6.2×10^{-7}	TemisFlow software lithology library
Evaporites (salt)	3	2160	1.0×10^8	1	6.1	1.0×10^{-8}	TemisFlow software lithology library
Conglomerates	34	2600	1.2×10^6	0.1	3.27	1.0×10^{-7}	TemisFlow software lithology library
Muschelkalk evaporites and limestones	28	2587.0	1.3×10^6	1	3.57	8.43×10^{-7}	TemisFlow software lithology library
Buntsandstein Group sandstones	11	2600	2.0×10^6	0.7	4.6	1.0×10^{-7}	TemisFlow software lithology library; Freyemark <i>et al.</i> (2017, 2019)
Dolomites	12	2540	1.3×10^6	1	5.5	8.0×10^{-7}	TemisFlow software lithology library; Freyemark <i>et al.</i> (2017, 2019)
Permo-Carboniferous sandstones	13	2600	5.0×10^5	1	4.6	1.0×10^{-7}	TemisFlow software lithology library; Freyemark <i>et al.</i> (2017, 2019)
Granite	21	2670	†	1	3.0	3.30×10^{-8}	TemisFlow software lithology library
Continental generic		2650	†		3.0	3.0×10^{-7}	TemisFlow software lithology library
Lower continental generic		2900	†		2.0	5.0×10^{-7}	TemisFlow software lithology library
Peridotite		3300	†		3.0	3.0×10^{-8}	TemisFlow software lithology library
Water			0.6				

The indexes correspond to the values given to each facies in the properties maps provided in the Supplementary Material files. *Zanis stands for the vertical anisotropy and the presented values are the multipliers used to obtain the vertical permeability.

†Granite, constant permeability of 0.005 mD; ‡no permeability.

meteoritic freshwaters, and then rise upwards to the basement–sediment interface at the Soultz and Landau geothermal sites (Sanjuan *et al.* 2010, 2016; Bossennec *et al.* 2021a). Convective behaviour is also reported as possible (Clauser and Villingier 1990; Sanjuan *et al.* 2010; Freymark *et al.* 2017) at the basement–sedimentary cover interface. The deep-basin convective cells allow flows of sedimentary brine up to horst structures (e.g. Soultz Horst). This scenario is consistent with thermal anomalies spotted along the URG (Soultz, Rittershoffen and Landau). It is specific to the area delimited by Strasbourg as the southern boundary and Darmstadt as the northern border (Fig. 1a). The substantial heterogeneity of the fault behaviour leads to local upwellings at the block (field) scale along several NE–SW-striking faults (Sanjuan *et al.* 2016). The geochemical signature of the fracture mineralization (Bossennec *et al.* 2021a) suggests a contribution from Cenozoic fluids and recent meteoric waters in Mesozoic and granitic basement aquifers. The potential connection between these scales remains uncertain because of the lack of data integration in a 3D basin-scale model. A significant contribution of south–north-directed flow below the Cenozoic Graben infill and along north–south-striking faults has

been shown by models in Koltzer *et al.* (2019b), indicating that oversimplified flow-path assumptions in 2D from east to west, as shown in Figure 1b, do not realistically capture the complex heat and mass transport in 3D.

Materials and methods

Basin modelling methodology applied to the geothermal field

Basin modelling is a predictive methodology that assesses the evolution of a sedimentary basin and associated thermal, geochemical and hydrodynamic processes (Ungerer *et al.* 1990; Schneider *et al.* 2000; Hantschel and Kauerauf 2009; Peters *et al.* 2017; Lemgruber-Traby *et al.* 2020b). Initially conceptualized for exploring hydrocarbon resources, basin modelling integrates a wide range of data, tests different scenarios and quantitatively models the effects of interdependent processes during basin evolution (Fig. 2). The main critical processes accessed with basin modelling are thermal and pressure related. The changes in

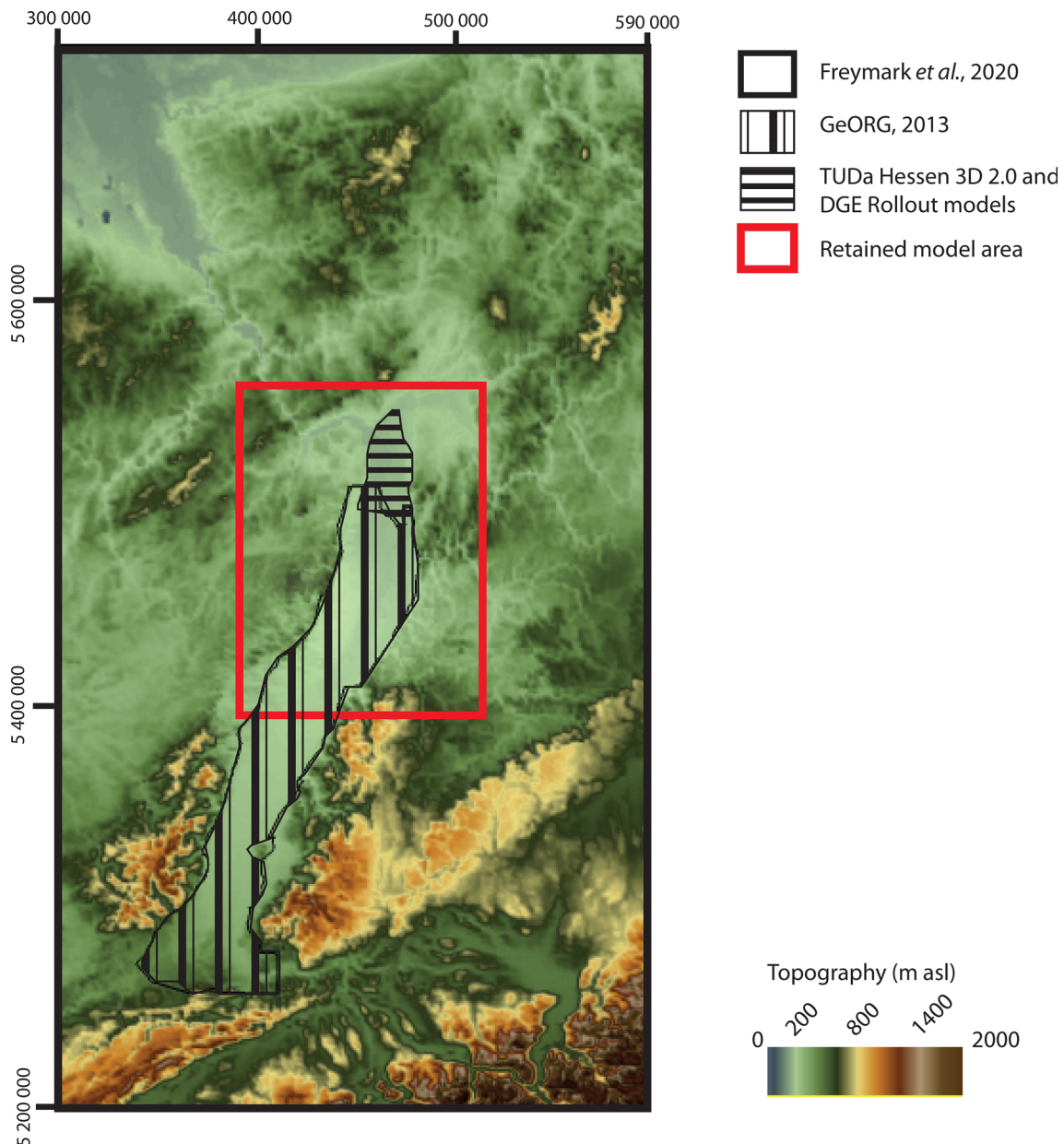


Fig. 3. Areal extent of the integrated structural models in the NURG region. m asl, metres above sea level.

Table 2. Implemented layers and associated lithofacies

Layer	Facies	Top age (Ma)	Source
Quaternary	Marl	0	
Young Tertiary	Marl	20	Torresan <i>et al.</i> 2021
Worms Formation	Map 1	20.44	Beccaletto <i>et al.</i> (2010)
Landau Formation	Map 1	23.03	Beccaletto <i>et al.</i> (2010)
Froidefontaine Formation	Marl	33.9	Beccaletto <i>et al.</i> (2010)
Pechelbronn Group	Map 2	37.8	Beccaletto <i>et al.</i> (2010)
Hiatus		66	
Dogger/Lias/Keuper	Marl	153	
Muschelkalk	Evaporites and carbonate	240	Beccaletto <i>et al.</i> (2010); Torresan <i>et al.</i> 2021
Buntsandstein Group	Sandstones	245	Torresan <i>et al.</i> 2021
Zechstein	Dolomites	253.8	Torresan <i>et al.</i> 2021
Permo-Carboniferous	Sandstones	279.3	Torresan <i>et al.</i> 2021
Basement	Granitoids, continental generic, lower continental generic, peridotite		Beccaletto <i>et al.</i> (2010)

For lithofacies properties, see Table 1. Maps 1 and 2 are presented in Figure 5.

petrophysical properties and pressure conditions drive hydrocarbon expulsion, migration and entrapment. Indeed, when interested in petroleum system evaluation, the thermal evolution is essential to understand the thermal cracking of source rocks and the evolution of hydrocarbon properties in the reservoirs. This study proposes deviating from the fossil energy application of basin modelling to investigate the geothermal pathways within the URG.

The thermal simulation performed in basin modelling integrates heat sources associated with sedimentation, erosion or intrusion, radiogenic heat generation, and both conductive and advective heat transfers (equation 1: modified from Lemgruber-Traby *et al.* 2020b). As for the hydrodynamic fluid circulation, the pressure differential and petrophysical properties are used within a Darcy-type law to calculate fluid-flow velocity and direction (equation 2). The main mechanisms responsible for the thermal structure of the URG (Baillieux *et al.* 2014; Armandine Les Landes *et al.* 2019) are then integrated into basin modelling simulations:

$$\frac{\partial}{\partial t}(\rho_s c_s T) + \text{div}(\rho_\alpha \Phi S_\alpha c_\alpha \vec{T} V_\alpha - \lambda_b \nabla T) = q_o + q_r \quad (1)$$

where T is the temperature; t is the time; Φ is porosity, which evolves with the effective stress (which approximates to the burial depth)

(Schneider *et al.* 1996) according to compaction curves defined for each facies (see Supplementary material Table S1); ρ is the density; c is the heat capacity; λ is the thermal conductivity – the thermal conductivity is calculated according to both rock matrix and water thermal conductivities (Table 1), taking into account the evolution of the sediments' porosity during basin evolution (Table S1); subscript α represents the fluid phase (water in this study) and subscript s represents the water-saturated porous media; q_r is the radioactivity heat source and q_o represents others heat sources, which may include heat sources linked to the sediment deposition or erosion, to magmatic intrusions or to the fluid volume variation by hydrocarbon generation.

\vec{V}_α is the velocity of phase α , obtained from Darcy's law generalized in a function of pressure:

$$\vec{U}_\alpha = \Phi(\vec{V}_\alpha - \vec{V}_s) = -\frac{\bar{K}}{\mu_\alpha}(\nabla P - \rho_\alpha \vec{g}) \quad (2)$$

where \vec{U}_α is the Darcy velocity; μ_α is the viscosity of phase α ; and \bar{K} is the permeability of the porous media, calculated according to a specific surface area using the Carman-Kozeny's approach (Table 1).

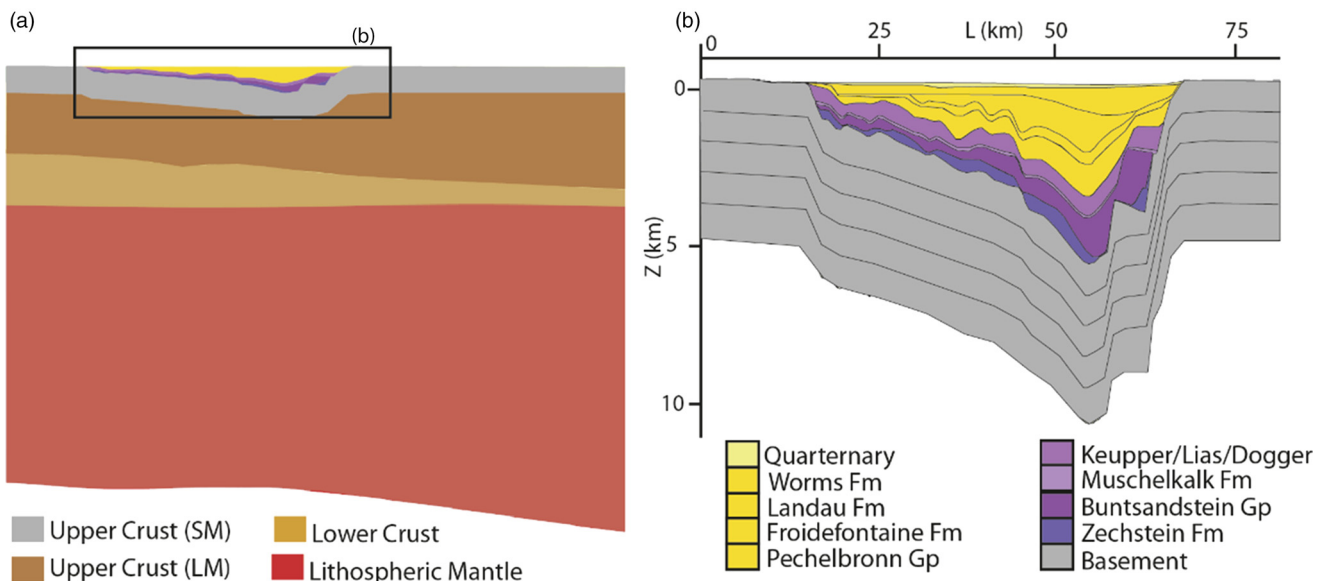


Fig. 4. (a) Coupled sedimentary and lithospheric models. (b) Focus on the sedimentary model, including the upper part of the upper crust. SM, sedimentary model; LM, lithospheric model.

Datasets and model definition

The presented 3D structural model results from an extensive data-integration process. The model extends over France and Germany, and the dataset is implemented in the UTM 32 zone coordinate system. It includes depths horizons and lithostratigraphic content from Freymark *et al.* (2017), TUDa Hessen 3D 2.0 and DGE Rollout models proprietary data for the northern part of the URG (Frey *et al.* 2021; Hintze *et al.* 2022), and data from the GeORG project (Beccaletto *et al.* 2010). These three data sources present different geographical coverage (Fig. 3) and stratigraphic resolution. Integration and selection work was necessary to unify these various datasets and to build a representative structural model of the NURG (Table 2). A preferential retention order was defined according to data confidence, following: (1) TUDa Hessen 3D 2.0 and DGE Rollout models (Frey *et al.* 2021; Hintze *et al.* 2022); (2) GeORG project (Beccaletto *et al.* 2010); and (3) Freymark *et al.* (2017).

The basin model implemented in TemisFlow software for this study presents a structured regular grid with a horizontal resolution of 500 m and an extension of 100 × 300 km. The model vertical resolution varies laterally according to the defined model geometry (Fig. 4). It consists of 11 sedimentary layers from the Permo-Carboniferous to the Quaternary, lying on the crystalline Hercynian basement (Table 2; Fig. 4). Thermal simulations also considered a

lithospheric model divided into three layers: the upper crust, lower crust and the lithospheric mantle. The geometry of this lithospheric model was built according to data given in Freymark *et al.* (2017, 2019). In the TemisFlow lithospheric model, no fluid circulation or compaction-pressure calculations were performed. In order to take into account the fractured basement and allow the fluid flow through the basement faults and fracture network to be modelled, five basement layers with a thickness of 1 km each were added at the base of the TemisFlow 'sedimentary' model (Fig. 4).

For each defined stratigraphic interval, the lithofacies distribution and associated properties were defined (Tables 1 and 2; Fig. 5; see also Supplementary material Table S1). Furthermore, as faults cannot be discretized and implicitly taken into account in structured models, they could only be modelled by defining particular fault facies in selected areas. These fault facies were defined with an equivalent fault thickness of 25 m by considering a porosity of 5% in the 500 m large cells, and with their permeabilities and locations varying in the different scenarios, as presented in Table 3.

Thermal boundary conditions

To constrain the thermal history of the basin, the upper thermal boundary (i.e. the surface temperature evolution) integrated the palaeolatitude and palaeoclimate evolution of the study area

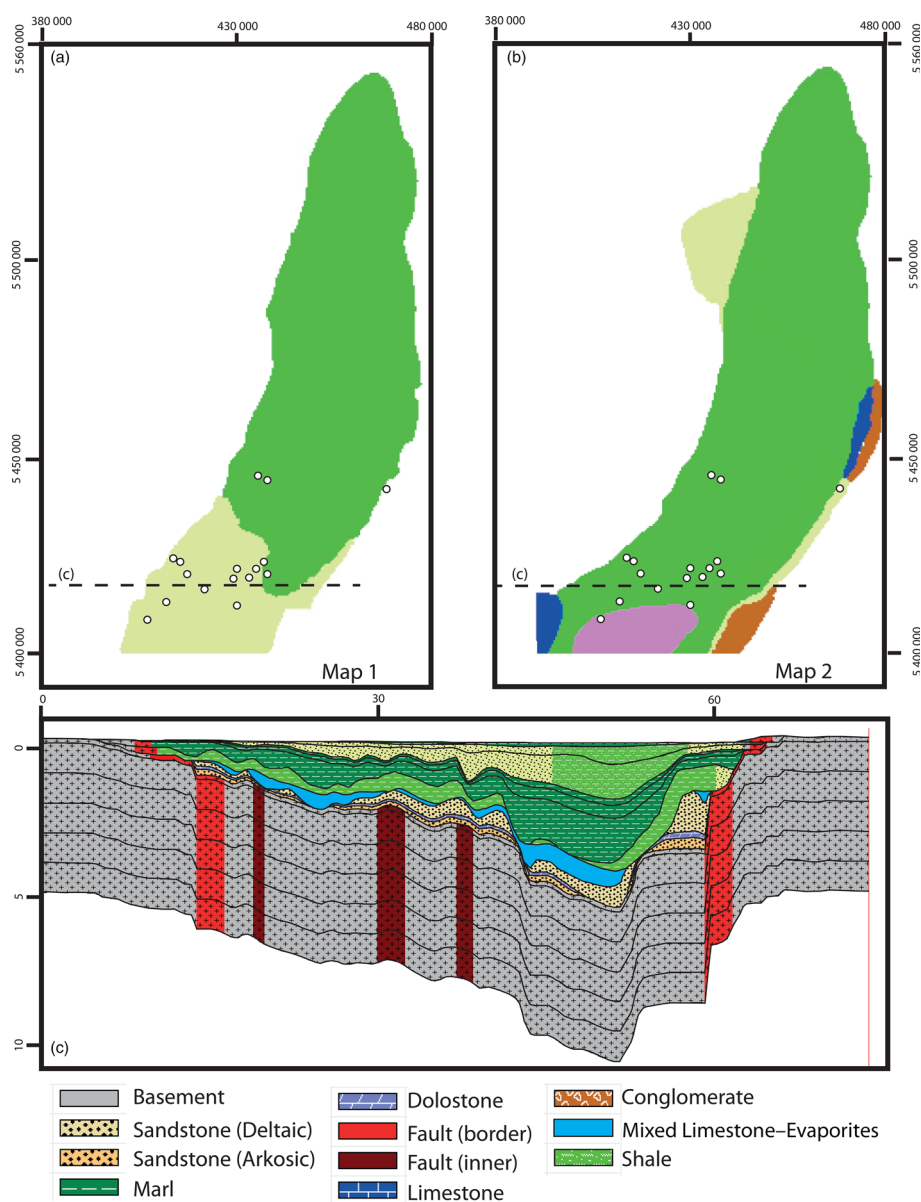
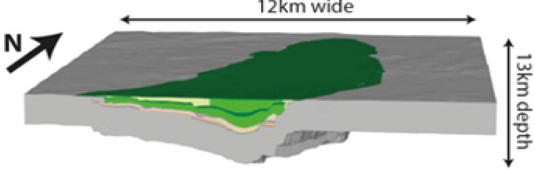
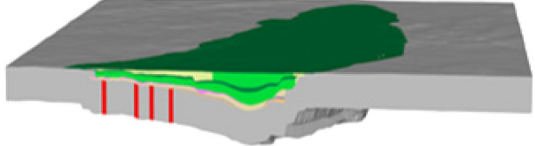
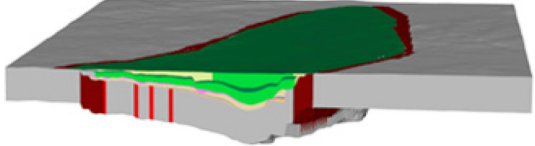
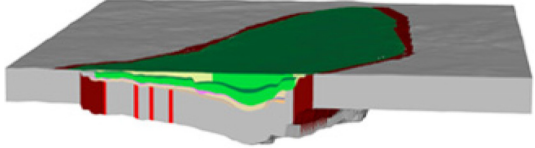
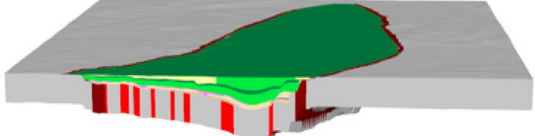


Fig. 5. Facies distribution maps assigned for (a) the Worms and Landau formations (Map 1) and (b) for the Pechelbronn Group (Map 2). The location of cross-section (c), which shows the resulting facies distribution, is presented in (a) and (b).

Table 3. Modelled scenarios 1–5, including fault parametrization and basement components

Scenario	Model geometry	Basement components	Permeability (mD)
1		Homogeneous basement (grey)	0.005
2		Heterogeneous basement and western inner fault system (red)	Basement, 0.005; red inner faults, 10
3		Heterogeneous basement: with western inner fault system (red) and major border faults (dark red)	Basement, 0.005; red inner faults, 5; dark red border faults, 10
4		Heterogeneous basement: with western inner fault system (red) and highly permeable major border faults (dark red)	Basement, 0.005; red inner faults, 5; dark red border faults, 50
5		Heterogeneous basement: with western inner fault system (red) and highly permeable major border faults (dark red)	Basement, 0.005; red inner faults, 5; dark red border faults, 50

(Scotese 1997; Matthews *et al.* 2016). The geometry of the isotherm corresponding to the lithosphere–asthenosphere interface was considered as the lower thermal boundary, with an evolution through time corresponding to the lithospheric model. This lithospheric model reproduced the main lithospheric processes, including the rifting event. The crust thermal model integrates the lithospheric mantle model fully coupled to the sedimentary basin model. The temperature evolution of the lithospheric model was impacted by lithology effects, high sedimentation rates, overpressures and boundary condition changes occurring in the sedimentary model. The evolution of heat flow through time was then influenced both by sedimentary processes and by rifting (Bourgeois *et al.* 2007). The model evolves from the Late Carboniferous to the Quaternary, including a rifting event that extended from 46 to 23 Ma. The rifting was based on a homogeneous thinning factor (McKenzie 1978) of 4 based on previous advanced basement modelling in the southern URG (Roussé 2006; Roussé *et al.* 2016). Erosion periods were not integrated into this first-order model because they are not necessary to directly calibrate the present-stage temperature model.

Modelled scenarios

Of all the simulations that were run to test hypotheses and analyse their impact on the thermal field, a set of five scenarios were finally retained, highlighting the influence of the graben structures on hydrodynamic and thermodynamic behaviour. The five scenarios presented in Table 3 allow the results for each parameter influencing the thermal field to be compared. The scenarios were constructed, tested and evolved step by step. The first scenario did not consider any fault or fractured areas. This scenario served as a starting point to allow calibration of the ‘background’ temperature in areas not affected by advective heat transfer and also served as an indicator of

areas in which advective heat transfer is important. In the second scenario, key permeable faults were defined in the basement (Fig. 6). The selection of these faults took into account the first calibration of Scenario 1 and focused on the Soultz and Landau areas, where a high density of faults have been mapped (Fig. 6). Scenario 3 also included the graben border faults in accordance with Guillou-Frottier *et al.* (2013), who demonstrated that these structural elements play an important role in the advective and convective circulation of fluid along the graben. In Scenario 4 the permeabilities associated with the basement hydraulic heterogeneity structures were modified to allow a better calibration with the available data. A final scenario (Scenario 5) integrated faults away from the Soultz and Landau areas. Knowing that the model resolution and type of grid do not allow consideration of all mapped faults, this scenario aimed to provide a suitable representation of the fault network and the entire modelled area; however, additional work would be necessary to define which faults are more pertinent to be considered.

Scenarios results and calibration

The model temperature results were compared with temperature data available for 16 wells (Supplementary material Table S2). Only five of the wells crossed the Buntsandstein Group sandstones and reached the fractured basement (deep wells in Fig. 7). For the other, shallow, wells, even though their temperature regime resulted mainly from conductive heat transfers, they were also impacted by changes in the scenarios related to water flow (Fig. 7). This influence was less than for the deep wells. The calculated temperatures obtained from the different scenarios for the shallow wells varied by about 10°C, whereas for the deep wells they varied by up to 50°C (Fig. 7), highlighting the influence of fault-related hydrothermal flow on the deep thermal field. Overall, calibration of

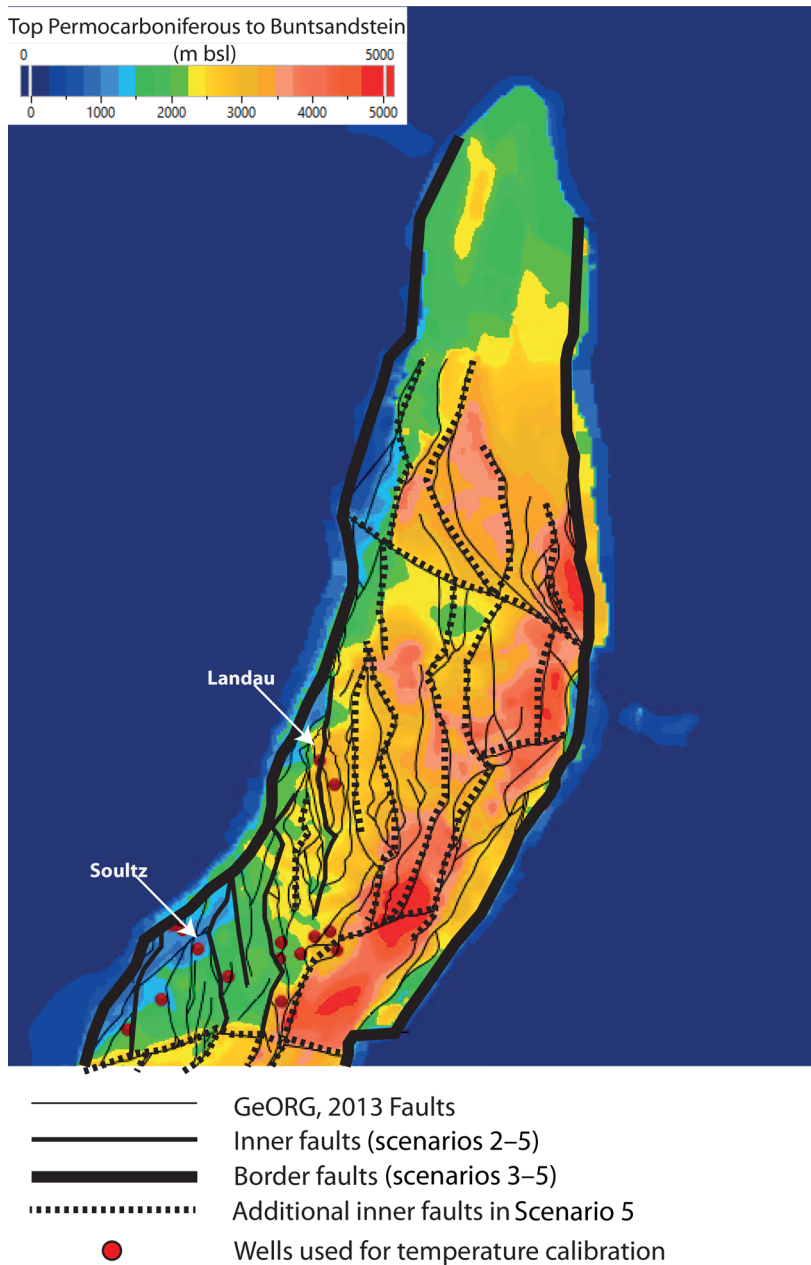


Fig. 6. The locations of the faults taken into account in the modelled scenarios. m bsl, metres below sea level.

the wells' temperature improved from Scenario 1 to Scenario 4. The calibration results for the well data change only slightly between scenarios 4 and 5; however, Scenario 5 shows more similarities with the GeORG project (Beccaletto *et al.* 2010) temperature maps for the top of Buntsandstein Group. Although these maps may not be considered as raw data that need to be fitted, these interpolation maps, which take the faults into account as discontinuities, serve as a good calibration indicator. This is especially helpful when far from the calibration wells used in this study.

The impact of water circulation on the temperature field of the Buntsandstein Group can be seen clearly in the results for the different scenarios (Fig. 8). When no preferential water circulation pathway is modelled within the basement (Scenario 1), the model temperature results for the western part of the Buntsandstein Group are considerably lower than for the other scenarios (Fig. 8). When accounting for the presence of permeable faults localized at the basin centre (scenarios 2–5), the water circulation causes a temperature increase in the surrounding rocks. However, when considering a meteoric water recharge from the graben shoulders that only occurs through the fractured basement (Scenario 2), the temperature increase is too great and the results overestimate the

temperature in the deep wells (Fig. 7). The interpretation of the presence of permeable faults at the borders of the graben (scenarios 3–5) would result in an inflow of meteoric cold water that cools down the deepest areas of the basement (Fig. 9), as also demonstrated in the models of Freymark *et al.* (2019) and Koltzer *et al.* (2019b). The water that flows upwards through the inner faults of the basin is consequently less hot than in previous scenarios, allowing a better temperature calibration.

Discussion

This study was performed mainly using publicly available regional data, except for the northern area where a more detailed proprietary interpretation was used. The modelled faults are oversimplified both in terms of representation and properties definition; however, it allows a good overview of the temperature distribution and the investigation of the mechanisms related to the thermal anomalies at the basin scale. The model temperature calibration relied only on raw data (i.e. temperature measurements) but in the study area only a few available borehole data are deep enough to reach depths greater than 2000 m.

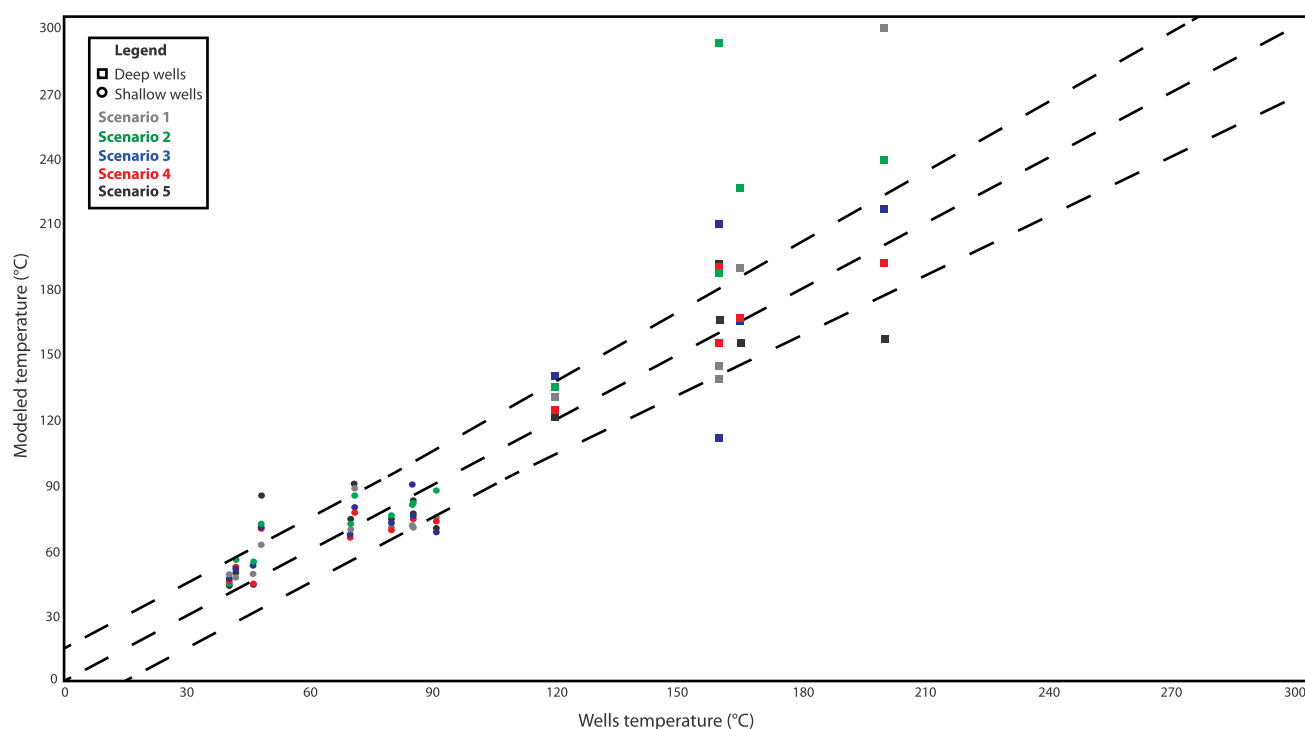


Fig. 7. Cross-plot of measured v. modelled temperatures for all scenarios. Error bars are 10°C when the measured temperatures are less than 100°C, and are 10% of the measure temperature otherwise.

In contrast to the models of Freymark *et al.* (2019) and Koltzer *et al.* (2019b), no particular piezometric conditions or water-head levels were defined in the model. The porous media and fractures are assumed to be saturated throughout the entire column, up to the model surface, which on the basin scale is sufficiently close to reality. The pressure differential that guides the fluid flow follows the differential topographical relief, which is defined by the topography map used as the model surface and which ranges from 100 to 850 m above sea level in the modelled area. When not considering the presence of permeable faults, the regional convective system is not initiated. Although the influence of the main border faults is key to explaining the recharge of the system and calibrating the model with the available data, the presence of inner faults alone allow the onset of a convection system. The locations of preferential recharge and discharge areas on the URG shoulders correspond to previous models (Armandine Les Landes *et al.* 2019; Freymark *et al.* 2019). The main recharge areas in this model are located south of Karlsruhe, south of Heidelberg and west of Landau, which are shown as areas 1, 2 and 3, respectively, in Figure 9. The low heat-flow values obtained in these areas correspond to the inflow of cold meteoric water. Conversely, areas with higher heat-flow values correspond to the upwelling of hotter water. These areas are located either at the vicinity of inner faults or along the border faults in areas with a lower altitude. The border fault systems thus play a double role of charge and discharge, as suspected in the 2D conceptual models (Cathelineau and Boiron 2010; Bossennec *et al.* 2021a). Within the main border faults, flow-velocity results range from 5×10^{-4} to 2×10^{-2} m/day, as proposed in the previous crustal models (Freymark *et al.* 2019).

The models' results show that the internal basement faults play an important role in focusing the upward water migration within the fractured basement. They are necessary to reproduce the fine-scale heterogeneities observed in the inner parts of the rift. Such fault mapping is complexified in the crystalline basement. The faults represented in the model were selected N00–N150 faults located in the vicinity of the available well data. As discussed previously, the

presented model allowed calibration of the gathered data and helped in understanding the regional mechanisms responsible for the thermal structure of the URG. A good fit of the temperature field and reproduction of the anomalies was achieved for the southwestern model region by calibrating the fault permeability in the first scenarios. Considering faults in the northern and eastern parts of the model resulted in a more heterogeneous temperature field far from the calibration data. The areas with high-temperature anomalies are the result of the focusing effect of the basement faults and may be favourable for geothermal exploration but further work is necessary to improve the model predictability in these areas where fewer deep wells are available for calibration.

The impact of fault properties within the sedimentary units on the redistribution of the hydrothermal flow was not addressed in this study. Since the effect of faults on fluid flow is highly dependent on the mechanical properties of the rock at the time of faulting, these sedimentary faults can have variable behaviour depending on their history. Additional work on the relative chronology of faulting relative to burial and diagenesis would be necessary to better evaluate their role and to integrate them into a regional model. However, the faults in the tight crystalline basement can be considered highly permeable, with potential heterogeneity due to a reduction in permeability related to later fluid circulation and fluid–rock interactions and an improvement in permeability due to fault reactivation and associated fracturing. In these tight rocks, fault zones with their highly fractured damage zones act as a drain for fluid flow by forming the backbone of the reservoir that allows hot fluids to flow upwards or parallel to the fault strike (Bossennec *et al.* 2022), while the fault core can act as a relative barrier. Also, lateral, vertical and temporal variations in the fault hydraulic properties have not been included in the present work. The integration of geomechanical studies to assess fault stress and associated properties such as slip and dilation tendency, as proposed in Armandine Les Landes *et al.* (2019), could provide interesting information for basin modelling studies. Ongoing developments that allow the faults to be implemented as implicit in the model grid (Woillez *et al.* 2017) is another possible way forward in this work.

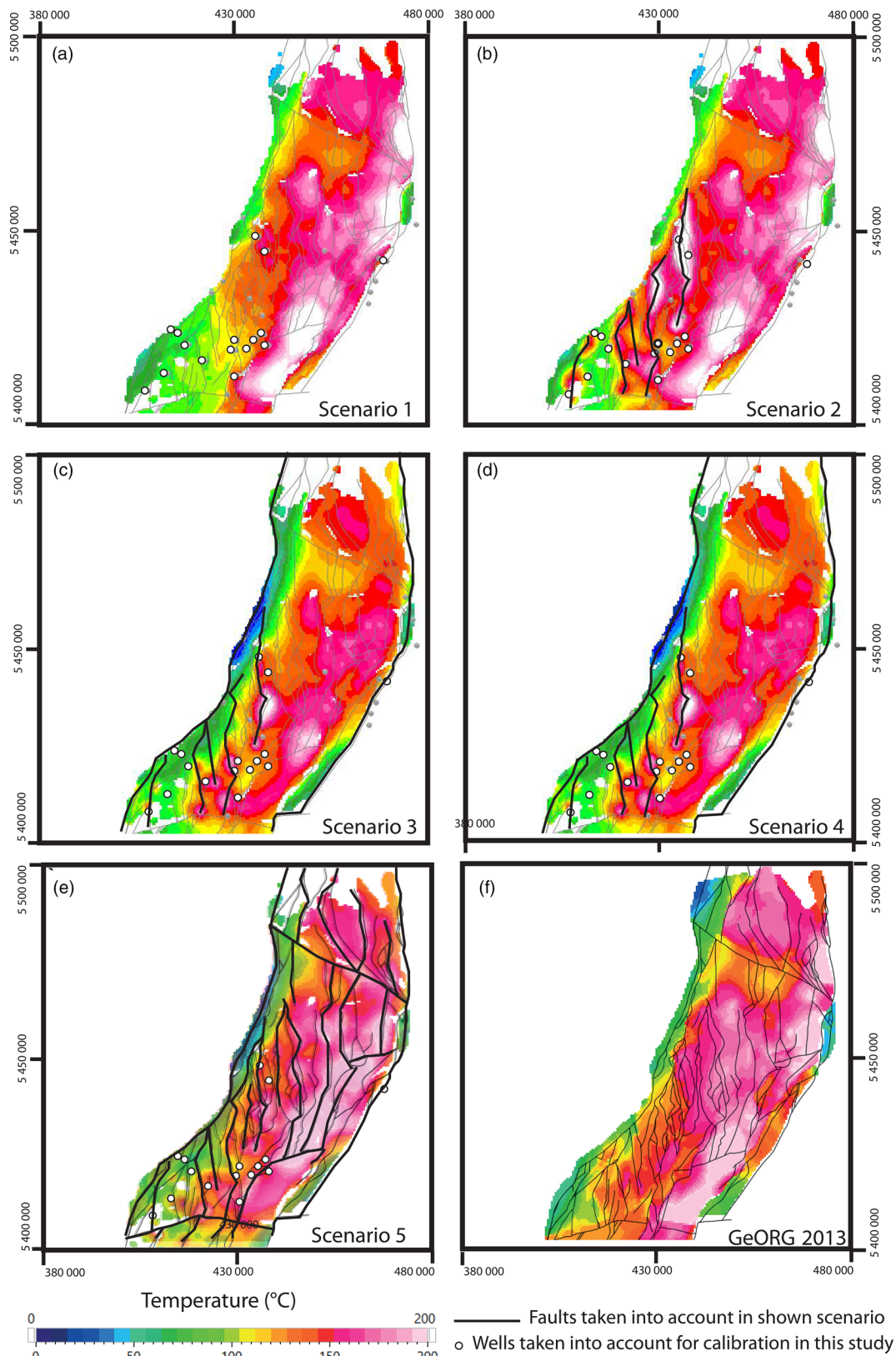


Fig. 8. Temperature maps for the top Buntsandstein Group for the five scenarios presented here: (a) Scenario 1, (b) Scenario 2, (c) Scenario 3, (d) Scenario 4 and (e) Scenario 5. (f) The temperatures obtained in GeORG 2013 (Beccaletto *et al.* 2010) for the top Buntsandstein Group.

As the evolution of the geothermal system plays an important role in fluid–rock interactions, and since the lithium lixiviation and concentration is a long process (Pogge von Strandmann *et al.* 2016), modelling the evolution of the geothermal system through geological time could help in better understanding the conditions of lithium enrichment of geothermal brines. As this study was

focused on understanding the present-day thermal structures, the focus was not stressed on detailing the information for the history of the evolution of the basin. A projected next step of this work would be to include information on the erosional phase in the Cretaceous (timing and eroded thickness distribution), topographical evolution and fault behaviour through time in the basin model. This would

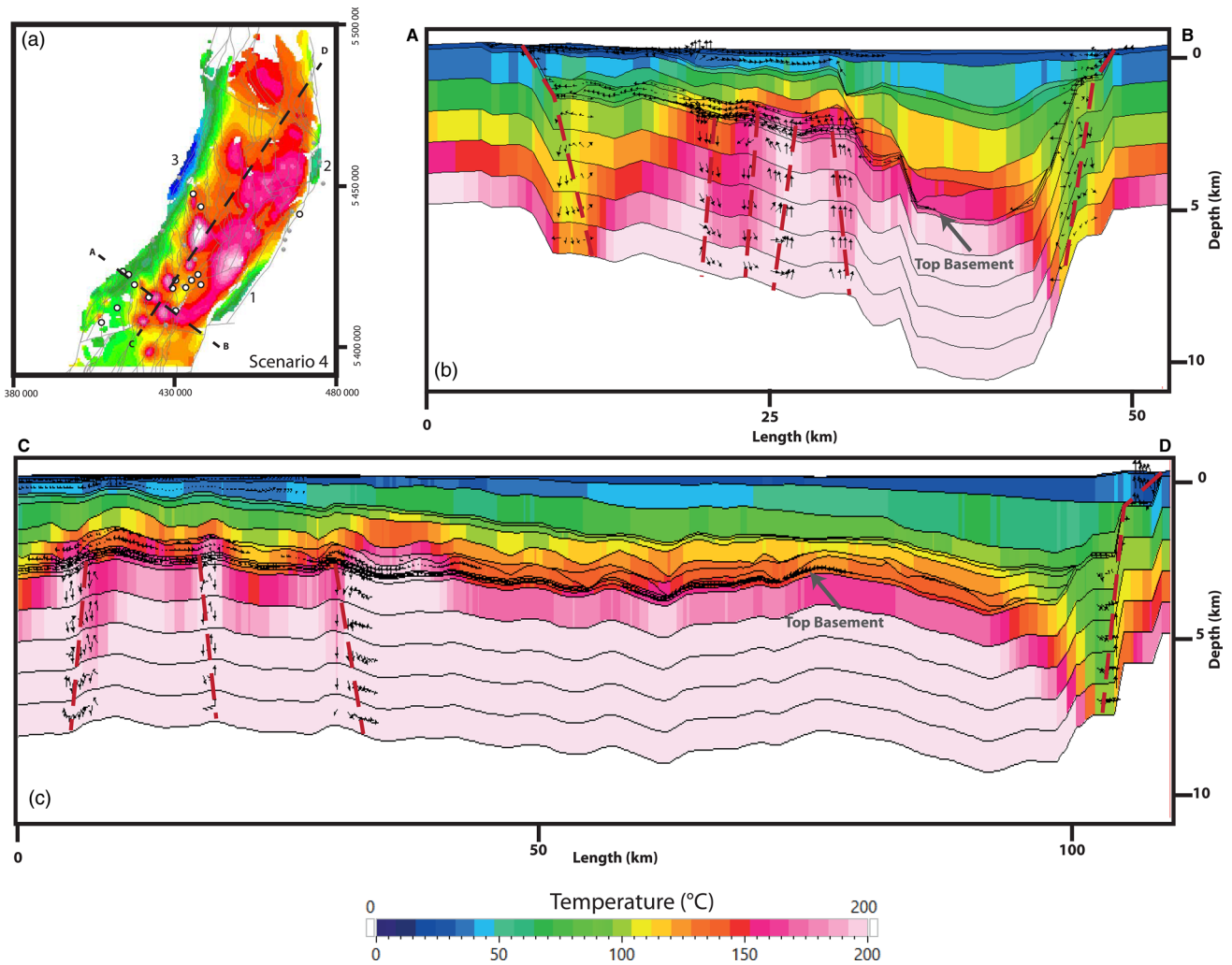


Fig. 9. (a) Temperature map of Scenario 4 at the top Buntsandstein Group layer, showing the locations of the cross-sections A–B and C–D presented in (b) and (c). (b) NW–SE cross-section of the model (A–B), with the temperature evolution and flow velocity represented by black vectors. (c) NNE–SSW cross-section of the model (C–D), with the temperature distribution and flow direction represented by black vectors. A lateral fluid flow that is globally northwards is modelled in the deep Permo-Triassic layers and at the top basement. The size of the arrows is a logarithmic representation of the water flow velocity.

allow the history of the geothermal system to be modelled and different scenarios tested to understand better the timing and location of favourable conditions for palaeofluid–rock interactions and the lithium enrichment of geothermal brines.

Conclusions

The basin modelling approach implemented in this study integrates a thermal field estimation, the variability of the thermal properties of the rocks and the hydraulic role of fault zones in a rift basin. The good fit with selected data and previous studies highlights that basin models can be a helpful tool to model and parametrize geothermal systems at the basin scale. Thus, this integrative approach reduces the uncertainty of the exploration phase in brownfields, particularly in the enhanced geothermal systems (EGS) targeted here. Conceptual models supposing a strong convection component in fault systems and the parametrization of internal faults are validated and necessary at the basin scale to reproduce the heterogeneous temperature field at geothermal reservoir depth. This output emphasizes the need to consider such structural elements and their complexity in geothermal system models. Resource assessments from the co-production of geothermal heat and mineral resources could also benefit from such a tool, given the perspective development of fluid–rock interactions schemes and their possible

implementation in such models. Fluid pathways can be mapped and the geothermal system analysis can be modelled during its entire geological history. Such an extended geological model improves the understanding of the physical processes governing such systems. This paves the road towards resource and reserve quantification and a potential assessment of their sustainability and renewability at the utilization timescale.

Acknowledgements We would like to thank the anonymous reviewers for the valuable comments and suggestions that helped improve the quality of the manuscript.

Author contributions AL-T: conceptualization (lead), methodology (equal), supervision (lead), validation (equal), writing – original draft (equal), writing – review & editing (equal); CB: conceptualization (equal), resources (lead), supervision (equal), validation (equal), writing – original draft (equal), writing – review & editing (equal); GB: data curation (lead), methodology (lead), validation (lead), writing – original draft (equal); CS: conceptualization (equal), methodology (equal), project administration (lead), supervision (equal), validation (equal), writing – review & editing (equal); RD: methodology (supporting), supervision (supporting), writing – review & editing (supporting); JvdV: data curation (equal), resources (equal), writing – review & editing (lead); KB: conceptualization (equal), project administration (equal), writing – review & editing (lead); IS: conceptualization (equal), project administration (equal), supervision (supporting), writing – review & editing (supporting).

Funding This research was co-funded by IFP Energies nouvelles (IFPEN) and integrated into the framework of the Interreg NWE Programme through the Roll-out of Deep Geothermal Energy in NW Europe (DGE-ROLLOUT) project (www.nweurope.eu/DGE-ROLLOUT). The Interreg NWE Programme is part of the European Cohesion Policy and is financed by the European Regional Development Funds (ERDF).

Competing interests The authors declare that they have no known competing financial interests or personal relationships that could have appeared to influence the work reported in this paper.

Data availability The datasets generated and analysed during this study are included in this published article and in its supplementary material files.

References

- Aquilina, L., Genter, A., Elsass, P. and Pribnow, D. 2000. Evolution of fluid circulation in the Rhine Graben: constraints from the chemistry of present fluids. In: Stober, I. and Bucher, K. (eds) *Hydrogeology of Crystalline Rocks*. Water Science and Technology Library, **34**. Springer, Dordrecht, The Netherlands, 177–203, https://doi.org/10.1007/978-94-017-1816-5_8
- Armandine Les Landes, A., Guillon, T., Peter-Borie, M., Blaisonneau, A., Rachez, X. and Gentier, S. 2019. Locating geothermal resources: insights from 3D stress and flow models at the upper Rhine Graben scale. *Geofluids*, **2019**, e8494539, <https://doi.org/10.1155/2019/8494539>
- Baillieux, P., Schill, E., Edel, J.-B. and Mauri, G. 2013. Localization of temperature anomalies in the upper Rhine Graben: insights from geophysics and neotectonic activity. *International Geology Review*, **55**, 1744–1762, <https://doi.org/10.1080/00206814.2013.794914>
- Baillieux, P., Schill, E., Abdelfettah, Y. and Dezayes, C. 2014. Possible natural fluid pathways from gravity pseudo-tomography in the geothermal fields of northern Alsace (Upper Rhine Graben). *Geotherm Energy*, **2**, 16, <https://doi.org/10.1186/s40517-014-0016-y>
- Bär, K.M. 2012. *Untersuchung der Tiefengeothermischen Potenziale von Hessen*. PhD thesis, Technische Universität, Darmstadt, Germany.
- Bär, K. and Sass, I. 2014. 3D-model of the deep geothermal potentials of Hesse (Germany) for enhanced geothermal systems. In: Proceedings of the Thirty-Ninth Workshop on Geothermal Reservoir Engineering, 24–26 February, Stanford, California, GP-TR-202, <https://pangea.stanford.edu/ERE/pdf/IGASTandard/SGW/2014/Bar.pdf>
- Bär, K., Reinsch, T. and Bott, J. 2020. The PetroPhysical property database (P³) – a global compilation of lab-measured rock properties. *Earth System Science Data*, **12**, 2485–2515, <https://doi.org/10.5194/essd-12-2485-2020>
- Beccaletto, L., Capar, L. *et al.* 2010. The GeORG project – seismic interpretation, structural pattern and 3D modelling of the Upper Rhine Graben – first scientific results. Presented at the Technical Workshop on Geopotential of the Upper Rhine Graben (GeORG), 18 November 2010, Freiburg, Germany.
- Berger, J.-P., Reichenbacher, B. *et al.* 2005. Eocene-pleiocene time scale and stratigraphy of the Upper Rhine Graben (URG) and the Swiss Molasse Basin (SMB). *International Journal of Earth Sciences (Geologische Rundschau)*, **94**, 711–731, <https://doi.org/10.1007/s00531-005-0479-y>
- Bertrand, L., Jusseume, J., Géraud, Y., Diraison, M., Damy, P.C., Navelot, V. and Haffen, S. 2018. Structural heritage, reactivation and distribution of fault and fracture network in a rifting context: case study of the western shoulder of the Upper Rhine Graben. *Journal of Structural Geology*, **108**, 243–255, <https://doi.org/10.1016/j.jsg.2017.09.006>
- Böcker, J., Littke, R. and Forster, A. 2017. An overview on source rocks and the petroleum system of the central Upper Rhine Graben. *International Journal of Earth Sciences (Geologische Rundschau)*, **106**, 707–742, <https://doi.org/10.1007/s00531-016-1330-3>
- Bossennec, C. 2019. *Evolution of Transfer Properties of Sandstones by Diagenesis and Deformation: Case Study on Buntsandstein Gp. Sandstones, Upper Rhine Graben*. PhD thesis, Université de Lorraine, Nancy, France.
- Bossennec, C., Géraud, Y., Böcker, J., Klug, B., Mattioni, L., Bertrand, L. and Moretti, I. 2021a. Characterisation of fluid flow conditions and paths in the Buntsandstein Gp. sandstones reservoirs, Upper Rhine Graben. *Bulletin de la Société Géologique de France*, **192**, 35, <https://doi.org/10.1051/bsgf/2021027>
- Bossennec, C., Géraud, Y. *et al.* 2021b. Evolution of diagenetic conditions and burial history in Buntsandstein Gp. fractured sandstones (Upper Rhine Graben) from in-situ $\delta^{18}\text{O}$ of Quartz and $^{40}\text{Ar}/^{39}\text{Ar}$ geochronology of K-feldspar overgrowths. *International Journal of Earth Sciences (Geologische Rundschau)*, **110**, 2779–2802, <https://doi.org/10.1007/s00531-021-02080-2>
- Bossennec, C., Seib, L., Frey, M., van der Vaart, J. and Sass, I. 2022. Structural architecture and permeability patterns of crystalline reservoir rocks in the northern Upper Rhine Graben: insights from surface analogues of the Odenwald. *Energies*, **15**, 1310, <https://doi.org/10.3390/en15041310>
- Bourgeois, O., Ford, M. *et al.* 2007. Separation of rifting and lithospheric folding signatures in the NW-Alpine foreland. *International Journal of Earth Sciences (Geologische Rundschau)*, **96**, 1003–1031, <https://doi.org/10.1007/s00531-007-0202-2>
- Cathelineau, M. and Boiron, M.-C. 2010. Downward penetration and mixing of sedimentary brines and dilute hot waters at 5 km depth in the granite basement at Soultz-Sous-Forêts (Rhine Graben, France). *Comptes Rendus Geoscience*, **342**, 560–565, <https://doi.org/10.1016/j.crte.2009.08.010>
- Clauser, C. and Villinger, H. 1990. Analysis of conductive and convective heat transfer in a sedimentary basin, demonstrated for the Rheingraben. *Geophysical Journal International*, **100**, 393–414, <https://doi.org/10.1111/j.1365-246X.1990.tb00693.x>
- Cloetingh, S., Cornu, T., Ziegler, P. and Beekman, F. 2006. Neotectonics and intraplate continental topography of the northern Alpine foreland. *Earth-Science Reviews*, **74**, 127–196, <https://doi.org/10.1016/j.earscirev.2005.06.001>
- Derer, C.E., Schumacher, M.E. and Schäfer, A. 2005. The Northern Upper Rhine Graben: basin geometry and early syn-rift tectono-sedimentary evolution. *International Journal of Earth Sciences (Geologische Rundschau)*, **94**, 640–656, <https://doi.org/10.1007/s00531-005-0515-y>
- Dezayes, C. and Lerouge, C. 2019. Reconstructing paleofluid circulation at the Hercynian basement/Mesozoic sedimentary cover interface in the Upper Rhine Graben. *Geofluids*, **2019**, 1–30, <https://doi.org/10.1155/2019/4849860>
- Dezayes, C., Lerouge, C., Ramboz, C. and Wille, G. 2013. Relative chronology of deep circulations within the fractured basement of the Upper Rhine Graben. Poster presented at the European Geothermal Congress (EGC 2013), 3–7 June 2013, Pisa, Italy.
- Dezayes, C., Lerouge, C., Sanjuan, B., Ramboz, C. and Brach, M. 2015. Toward a better understanding of the fluid circulation in the Rhine Graben for a better geothermal exploration of the deep basins. In: Proceedings of the World Geothermal Congress, 16–24 April 2015, Australia–New Zealand. International Geothermal Association, Melbourne, Australia, 19–25.
- Dezayes, C., Lerouge, C., Innocent, C. and Lach, P. 2021. Structural control on fluid circulation in a graben system: constraints from the Saint Pierre Bois Quarry (Vosges, France). *Journal of Structural Geology*, **146**, 104323, <https://doi.org/10.1016/j.jsg.2021.104323>
- Dezes, P., Schmid, S.M. and Ziegler, P.A. 2004. Evolution of the European Cenozoic rift system: interaction of the Alpine and Pyrenean orogens with their foreland lithosphere. *Tectonophysics*, **389**, 1–33, <https://doi.org/10.1016/j.tecto.2004.06.011>
- Dresmann, H., Keulen, N., Timar-Geng, Z., Fügenschuh, B., Wetzel, A. and Stünitz, H. 2010. The south-western Black Forest and the Upper Rhine Graben Main Border Fault: thermal history and hydrothermal fluid flow. *International Journal of Earth Sciences (Geologische Rundschau)*, **99**, 285–297, <https://doi.org/10.1007/s00531-008-0391-3>
- Edel, J.-B., Schulmann, K. and Rotstein, Y. 2007. The Variscan tectonic inheritance of the Upper Rhine Graben: evidence of reactivations in the Lias, Late Eocene–Oligocene up to the recent. *International Journal of Earth Sciences*, **96**, 305–325, <https://doi.org/10.1007/s00531-006-0092-8>
- Frey, M., Weinert, S., Bär, K., van der Vaart, J., Dezayes, C., Calcagno, P. and Sass, I. 2021. Integrated 3D geological modelling of the northern Upper Rhine Graben by joint inversion of gravimetry and magnetic data. *Tectonophysics*, **813**, 228927, <https://doi.org/10.1016/j.tecto.2021.228927>
- Frey, M., Sippel, J., Scheck-Wenderoth, M., Bär, K., Stiller, M., Fritsche, J.-G. and Kracht, M. 2017. The deep thermal field of the Upper Rhine Graben. *Tectonophysics*, **694**, 114–129, <https://doi.org/10.1016/j.tecto.2016.11.013>
- Frey, M., Bott, J., Cacace, M., Ziegler, M. and Scheck-Wenderoth, M. 2019. Influence of the main border faults on the 3D hydraulic field of the central Upper Rhine Graben. *Geofluids*, **2019**, 1–21, <https://doi.org/10.1155/2019/7520714>
- Gentier, S., Rachez, X., Ngoc, T.D.T., Peter-Borie, M. and Souque, C. 2010. 3D flow modelling of the medium-term circulation test performed in the deep geothermal site of Soultz-Sous-Forêts (France). In: Proceedings of the World Geothermal Congress 2010, 25–29 April, Bali, Indonesia. International Energy Agency (IEA), Paris, 13.
- Glaas, C., Vidal, J. and Genter, A. 2021. Structural characterization of naturally fractured geothermal reservoirs in the central Upper Rhine Graben. *Journal of Structural Geology*, **148**, 104370, <https://doi.org/10.1016/j.jsg.2021.104370>
- Guillou-Frottier, L., Carré, C., Bourguin, B., Bouchot, V. and Genter, A. 2013. Structure of hydrothermal convection in the Upper Rhine Graben as inferred from corrected temperature data and basin-scale numerical models. *Journal of Volcanology and Geothermal Research*, **256**, 29–49, <https://doi.org/10.1016/j.jvolgeores.2013.02.008>
- Guillou-Frottier, L., Duwiquet, H., Launay, G., Taillefer, A., Roche, V. and Link, G. 2020. On the morphology and amplitude of 2D and 3D thermal anomalies induced by buoyancy-driven flow within and around fault zones. *Solid Earth*, **11**, 1571–1595, <https://doi.org/10.5194/se-11-1571-2020>
- Haffen, S., Géraud, Y. and Diraison, M. 2015. Geothermal, structural and petrophysical characteristics of Buntsandstein sandstone reservoir (Upper Rhine Graben, France). In: Proceedings of the World Geothermal Congress, 16–24 April 2015, Australia–New Zealand. International Geothermal Association, Melbourne, Australia, 11p.
- Hantschel, T. and Kauerauf, A.I. 2009. *Fundamentals of Basin and Petroleum Systems Modeling*. Springer, Berlin.
- Hintze, M., Bär, K., Bott, J. and Sass, I. 2022. Geological–Geothermal 3D Model of the Cenozoic Graben Fill of the Northern Upper Rhine Graben, Germany. Technische Universität Darmstadt, Darmstadt, Germany, <https://tudatalib.ulb.tu-darmstadt.de/handle/tudatalib/3403> [last accessed 11 August 2022].
- Illies, J.H. 1972. The Rhine Graben rift system – plate tectonics and transform faulting. *Geophysical Surveys*, **1**, 27–60, <https://doi.org/10.1007/BF01449550>

- Koltzer, N., Scheck-Wenderoth, M. *et al.* 2019a. The effects of regional fluid flow on deep temperatures (Hesse, Germany). *Energies*, **12**, 2081, <https://doi.org/10.3390/en12112081>
- Koltzer, N., Scheck-Wenderoth, M., Cacace, M., Frick, M. and Bott, J. 2019b. Regional hydraulic model of the Upper Rhine Graben. *Advances in Geosciences*, **49**, 197–206, <https://doi.org/10.5194/adgeo-49-197-2019>
- Lemgruber-Traby, A., Bonte, D. and Souque, C. 2020a. Thermal assessment of Los Humeros geothermal system through basin modeling. In: Proceedings of the World Geothermal Congress 2020+1, Reykjavik. European Geothermal Energy Council, Brussels, <https://www.geothermal-energy.org/pdf/IGAstandard/WGC/2020/11060.pdf>
- Lemgruber-Traby, A., Espurt, N., Souque, C., Henry, P., Calderon, Y., Baby, P. and Brusset, S. 2020b. Thermal structure and source rock maturity of the North Peruvian forearc system: insights from a subduction–sedimentation integrated petroleum system modeling. *Marine and Petroleum Geology*, **122**, 104664, <https://doi.org/10.1016/j.marpetgeo.2020.104664>
- Lopes Cardozo, G.G.O. and Behrmann, J.H. 2006. Kinematic analysis of the Upper Rhine Graben boundary fault system. *Journal of Structural Geology*, **28**, 1028–1039, <https://doi.org/10.1016/j.jsg.2006.03.010>
- Lucazeau, F. and Vasseur, G. 1989. Heat flow density data from France and surrounding margins. *Tectonophysics*, **164**, 251–258, [https://doi.org/10.1016/0040-1951\(89\)90018-8](https://doi.org/10.1016/0040-1951(89)90018-8)
- Lutz, H., Kaulfuss, U. *et al.* 2010. Eckfeld Maar: window into an Eocene terrestrial habitat in central Europe. *Acta Geologica Sinica – English Edition*, **84**, 984–1009, <https://doi.org/10.1111/j.1755-6724.2010.00237.x>
- Lutz, H., Lorenz, V., Engel, T., Häfner, F. and Haneke, J. 2013. Paleogene phreatomagmatic volcanism on the western main fault of the Northern Upper Rhine Graben (Kisselwörth Diatreme and Nierstein–Asthaim Volcanic System, Germany). *Bulletin of Volcanology*, **75**, 741, <https://doi.org/10.1007/s00445-013-0741-2>
- Matthews, K.J., Maloney, K.T., Zahirovic, S., Williams, S.E., Seton, M. and Müller, R.D. 2016. Global plate boundary evolution and kinematics since the late Paleozoic. *Global and Planetary Change*, **146**, 226–250, <https://doi.org/10.1016/j.gloplacha.2016.10.002>
- McKenzie, D. 1978. Some remarks on the development of sedimentary basins. *Earth and Planetary Science Letters*, **40**, 25–32, [https://doi.org/10.1016/0012-821X\(78\)90071-7](https://doi.org/10.1016/0012-821X(78)90071-7)
- Meulenkamp, J.E. and Sissingh, W. 2003. Tertiary palaeogeography and tectonostratigraphic evolution of the Northern and Southern Peri-Tethys platforms and the intermediate domains of the African–Eurasian convergent plate boundary zone. *Palaeogeography, Palaeoclimatology, Palaeoecology*, **196**, 209–228, [https://doi.org/10.1016/S0031-0182\(03\)00319-5](https://doi.org/10.1016/S0031-0182(03)00319-5)
- Peters, K.E., Schenk, O., Hosford Scheirer, A., Wygrala, B. and Hantschel, T. 2017. Basin and petroleum system modeling. In: Hsu, C.S. and Robinson, P.R. (eds) *Springer Handbook of Petroleum Technology*. Springer Handbooks. Springer International, Cham, Switzerland, 381–417, https://doi.org/10.1007/978-3-319-49347-3_11
- Pogge von Strandmann, P.A.E., Burton, K.W., Opfergelt, S., Eiríksdóttir, E.S., Murphy, M.J., Einarsson, A. and Gislason, S.R. 2016. The effect of hydrothermal spring weathering processes and primary productivity on lithium isotopes: Lake Myvatn, Iceland. *Chemical Geology*, **445**, 4–13, <https://doi.org/10.1016/j.chemgeo.2016.02.026>
- Pribnow, D. and Schellschmidt, R. 2000. Thermal tracking of upper crustal fluid flow in the Rhine graben. *Geophysical Research Letters*, **27**, 1957–1960, <https://doi.org/10.1029/2000GL008494>
- Reicherter, K., Fritzsche, N. *et al.* 2008. Alpine tectonics north of the Alps. In: McCann, T. (ed.) *The Geology of Central Europe Volume 2: Mesozoic and Cenozoic*. Geological Society, London, 1233–1285, <https://doi.org/10.1144/CEV2P.7>
- Reinecker, J., Hochschild, T., Kraml, M., Löschan, G. and Kreuter, H. 2019. Experiences and challenges in geothermal exploration in the Upper Rhine Graben. In: Proceedings of the European Geothermal Congress 2019. European Geothermal Energy Council, Brussels, 11–12, <http://europeangeothermalcongress.eu/wp-content/uploads/2019/07/307.pdf>
- Rotstein, Y. and Schaming, M. 2008. Tectonic Implications of faulting styles along a rift margin: the boundary between the Rhine Graben and the Vosges mountains. *Tectonics*, **27**, TC2001, <https://doi.org/10.1029/2007TC002149>
- Rotstein, Y., Edel, J.-B., Gabriel, G., Boulanger, D., Schaming, M. and Munsch, M. 2006. Insight into the structure of the Upper Rhine Graben and its basement from a new compilation of Bouguer Gravity. *Tectonophysics*, **425**, 55–70, <https://doi.org/10.1016/j.tecto.2006.07.002>
- Roussé, S. 2006. *Architecture et Dynamique Des Séries Marines et Continentales de l'oligocène Moyen et Supérieur Du Sud Du Fossé Rhénan: Evolution Des Milieux de Dépôt En Contexte de Rift En Marge de l'avant-Pays Alpin*. PhD thesis, Université Louis Pasteur, Strasbourg, France.
- Roussé, S., Filleaudeau, P.-Y., Mermey, G.C., Letteron, A. and Schaming, M. 2016. Integrated stratigraphic and petroleum system modeling study of the Southern Upper Rhine Graben. In: *International Conference and Exhibition, Barcelona, Spain, 3–6 April 2016*. Society of Exploration Geophysicists, Houston, TX, 35–35, <https://doi.org/10.1190/ice2016-6491658.1>
- Sanjuan, B., Millot, R., Dezayes, C. and Brach, M. 2008. Fluid origin and circulation in the heat exchanger of Ets (France) estimated using geochemical and tracer test data. Paper presented at the EHDRA Scientific Conference, 24–25 September 2008, Soultz-sous-Forêt, France, hal-00773163
- Sanjuan, B., Millot, R., Dezayes, C. and Brach, M. 2010. Main characteristics of the deep geothermal brine (5 km) at Soultz-Sous-Forêts (France) determined using geochemical and tracer test data. *Comptes Rendus Geoscience*, **342**, 546–559, <https://doi.org/10.1016/j.crte.2009.10.009>
- Sanjuan, B., Millot, R., Innocent, C., Dezayes, C., Scheiber, J. and Brach, M. 2016. Major geochemical characteristics of geothermal brines from the Upper Rhine Graben granitic basement with constraints on temperature and circulation. *Chemical Geology*, **428**, 27–47, <https://doi.org/10.1016/j.chemgeo.2016.02.021>
- Schneider, F., Potdevin, J.L., Wolf, S. and Faille, I. 1996. Mechanical and tectonic compaction model for sedimentary basin simulators. *Tectonophysics*, **263**, 307–317, [https://doi.org/10.1016/S0040-1951\(96\)00027-3](https://doi.org/10.1016/S0040-1951(96)00027-3)
- Schneider, F., Wolf, S., Faille, I. and Pot, D. 2000. A 3d basin model for hydrocarbon potential evaluation: application to Congo offshore. *Oil & Gas Science and Technology – Revue IFP*, **55**, 3–13, <https://doi.org/10.2516/ogst:2000001>
- Schumacher, M.E. 2002. Upper Rhine Graben: role of preexisting structures during rift evolution. *Tectonics*, **21**, <https://doi.org/10.1029/2001TC900022>
- Scotese, C. 1997. Paleogeographic Atlas and Plate Tectonic Software. PALEOMAP Project, Arlington, TX.
- Sissingh, W. 1998. Comparative Tertiary stratigraphy of the Rhine Graben, Bresse Graben and Molasse basin: correlation of Alpine foreland events. *Tectonophysics*, **300**, 249–284, [https://doi.org/10.1016/S0040-1951\(98\)00243-1](https://doi.org/10.1016/S0040-1951(98)00243-1)
- Skrzypek, E. 2011. *Contribution Structurale, Pétrologique et Géochronologique à la Tectonique Intracontinentale de la Chaîne Hercynienne d'Europe (Sudètes, Vosges)*. PhD thesis, Université de Strasbourg, Strasbourg, France.
- Timar-Geng, Z., Fügenschuh, B., Wetzel, A. and Dresmann, H. 2006. Low-temperature thermochronology of the flanks of the southern Upper Rhine Graben. *International Journal of Earth Sciences (Geologische Rundschau)*, **95**, 685–702, <https://doi.org/10.1007/s00531-005-0059-1>
- Torresan, F., Piccinini, L., Cacace, M., Pola, M., Zampieri, D. and Fabbri, P. 2021. Numerical modeling as a tool for evaluating the renewability of geothermal resources: the case study of the Euganean geothermal system (NE Italy). *Environmental Geochemistry and Health*, **44**, 2135–2162, <https://doi.org/10.1007/s10653-021-01028-4>
- Ungerer, P., Burrus, J., Doligez, B., Chénet, P.Y. and Bessis, F. 1990. Basin evaluation by integrated two-dimensional modeling of heat transfer, fluid flow, hydrocarbon generation, and migration. *AAPG Bulletin*, **74**, 309–335, <https://doi.org/10.1306/0C9B22DB-1710-11D7-8645000102C1865D>
- Vidal, J. and Genter, A. 2018. Overview of naturally permeable fractured reservoirs in the Central and Southern Upper Rhine Graben: insights from geothermal wells. *Geothermics*, **74**, 57–73, <https://doi.org/10.1016/j.geothermics.2018.02.003>
- Vidal, J., Genter, A. and Schmittbuhl, J. 2015. How do permeable fractures in the Triassic sediments of Northern Alsace characterize the top of hydrothermal convective cells? Evidence from Soultz Geothermal Boreholes (France). *Geothermal Energy*, **3**, 8, <https://doi.org/10.1186/s40517-015-0026-4>
- Wuillez, M.-N., Souque, C., Rudkiewicz, J.-L., Willien, F. and Cornu, T. 2017. Insights in fault flow behaviour on onshore Nigeria petroleum system modelling. *Oil & Gas Science and Technology – Revue IFP Energies Nouvelles*, **72**, 31, <https://doi.org/10.2516/ogst/2017029>
- Ziegler, P.A. 1987. Late Cretaceous and Cenozoic intra-plate compressional deformations in the Alpine foreland – a geodynamic model. *Tectonophysics*, **137**, 389–420, [https://doi.org/10.1016/0040-1951\(87\)90330-1](https://doi.org/10.1016/0040-1951(87)90330-1)
- Ziegler, P.A. 1992. European Cenozoic rift system. *Tectonophysics*, **208**, 91–111, [https://doi.org/10.1016/0040-1951\(92\)90338-7](https://doi.org/10.1016/0040-1951(92)90338-7)
- Ziegler, P.A. and Dèzes, P. 2007. Cenozoic uplift of Variscan massifs in the Alpine foreland: timing and controlling mechanisms. *Global and Planetary Change*, **58**, 237–269, <https://doi.org/10.1016/j.gloplacha.2006.12.004>